Available online at www.sciencedirect.com
SCIENCE DIRECT®
International Journal of Mass Spectrometry 240 (2005) 273–284
International Journal of Mass Spectrometry
www.elsevier.com/locate/ijms

Is it biologically relevant to measure the structures of small peptides in the gas-phase?

Perdita E. Barran[a,*], Nick C. Polfer[a,1], Dominic J. Campopiano[a], David J. Clarke[a], Patrick R.R. Langridge-Smith[a], Ross J. Langley[b], John R.W. Govan[b], Alison Maxwell[c], Julia R. Dorin[c], Robert P. Millar[d], Michael T. Bowers[e]

[a] *School of Chemistry, University of Edinburgh, West Mains Road, Edinburgh EH9 3JJ, UK*
[b] *Department of Medical Microbiology, University Medical School, University of Edinburgh, Edinburgh EH8 9AG, UK*
[c] *MRC Human Genetics Unit, Western General Hospital, Edinburgh EH4 2XU, UK*
[d] *MRC Human Reproductive Sciences Unit, Centre for Reproductive Biology, The Chancellors Building, Edinburgh EH16 4SB, UK*
[e] *Department of Chemistry and Biochemistry, University of California, Santa Barbara, CA 93106-9510, USA*

Received 15 September 2004; accepted 27 September 2004
Available online 10 November 2004

Abstract

Recent developments in sample introduction of biologically relevant molecules have heralded a new era for gas-phase methods of structural determination. One of the biggest challenges is to relate gas-phase structures, often measured in the absence of water and counter ions, with in vivo biologically active structures. An advantage of gas-phase based techniques is that a given peptide can be analysed in a variety of different forms, for example, as a function of charge state, or with additional water molecules. Molecular modelling can provide insight into experimental findings and help elucidate the differences between structural forms. Combining experiment and theory provides a thorough interrogation of candidate conformations. Here two important naturally occurring peptide systems have been examined in detail and results are assessed in terms of their biological significance.

The first of these is gonadotropin-releasing hormone (GnRH), a decapeptide which is the central regulator of the reproductive system in vertebrates. We have examined several naturally occurring variants of this peptide using Ion Mobility Mass Spectrometry and Electron Capture Dissociation (ECD) in conjunction with Fourier Transform Ion Cyclotron Mass Spectrometry (FT-ICR-MS). Candidate conformations are modelled using the AMBER force field. Single amino acid changes, for example Gly6 → Ala6, or Ala6 → D-Ala6, have observable effects on the gas phase structure of GnRH. It has been shown that evolutionary primary sequence variations are key to the biological activity of GnRH, and it is thought that this is due to different binding affinities at target receptors. This work provides strong evidence that this activity is structurally based. The second system examined is the relationship between the quaternary structure and activity of two novel β-defensins. FT-ICR mass spectrometry has been employed to characterize di-sulphide bridging and dissociation based experiments utilised to investigate their structural core. Defr1, with five cysteines, exists as a covalently bound disulphide linked dimer; Defr1 Y5C with six cysteines also is observed as a dimer, but non-covalently bound, suggesting that this defensin has a tendency to aggregate. The activity of Defr1 is 10 times higher than that of Defr1 Y5C when tested against the pathogen *Pseudomonas aeruginosa*. The results from these studies could inform future design of novel GnRH type ligands and anti-microbial agents, and illustrate the power of gas-phase based techniques for solving peptide structures.

Keywords: Ion mobility; Peptides; ECD; FT-ICR

1. Introduction

Advances in proteomic technologies, coupled with the sequencing of the human genome have resulted in vast numbers of peptide ions being ‘measured’ daily in mass

* Corresponding author. Tel.: +44 131 650 7533; fax: +44 131 650 7533.
E-mail address: perdita.barran@ed.ac.uk (P.E. Barran).
[1] Present address: FOM Institute for Plasma Physics ‘Rijnhuizen’, Edisonbaan 14, 3430 BE Nieuwegein, The Netherlands.

1387-3806/$ – see front matter © 2004 Elsevier B.V. All rights reserved.
doi:10.1016/j.ijms.2004.09.013

spectrometers across the world [1]. Determination of the primary sequences of proteins expressed from cells is providing many research groups with a wealth of information. However, these high-throughput gas-phase techniques which analyse small proteolytic peptide fragments, do not yet provide information about secondary or tertiary structure. Clemmer and co-workers [2] have made some advances in that direction by employing ion mobility mass spectrometry, coupled with LC-analysis. This approach generates very large three-dimensional (3D) data sets which contain elution time, mass to charge ratios and drift times, where peptides that may exhibit homogeneous properties in one dimension, are distinguishable in another [3]. In order to relate the drift time to structure(s), it is necessary to perform calculations and compare the cross-sections of minimised low energy structures to those measured experimentally [4], which often can become a rate limiting step in such measurements. Unfortunately, information about the structure of these enzymatically digested fragments has little biological relevance. What is potentially more meaningful is to use gas-phase technologies, albeit at a lower throughput, to determine secondary and tertiary structures of peptides [5]. As with larger proteins, three-dimensional structures of small peptides are traditionally deduced either by such techniques as X-ray diffraction and nuclear magnetic resonance (NMR) or by theoretical prediction methods. Because of their size, the interplay between solvent/solute and internal interactions enables peptides to be more flexible than proteins. Nevertheless, the secondary structure(s) of peptides, arising in part from this conformational flexibility, are important. Significantly different pharmacological ligand/receptor activities testify for single-point mutations of peptides [6]. NMR and crystallography are notoriously difficult to apply to small peptide systems due to their inherent flexibility. Hence, active form(s) are often difficult to isolate. Computational approaches are gaining momentum as viable methods to determine tertiary structures [7]. However, much effort has been (rightly) directed to model systems [8], and only a handful of small real peptide systems have been solved using solely in silico techniques which then rely on comparison to experimental data [9,10].

The gas-phase offers a different environment for studying the conformations of peptide molecules. Time scales available for study are several magnitudes smaller than those present in NMR, and the ability to alter the energy available to the isolated gas phase ion means that conformational flexibility may be examined in great detail. Furthermore since the dielectric constant of a vacuum ($\varepsilon_{vacuum} = 1$) is more similar to the immediate environment of a membrane receptor ($\varepsilon_{peptide/protein} = 2$–$4$) than for water ($\varepsilon_{water} = 80$), [11] the gas-phase is an appropriate 'medium' in which to study the structures of peptides which in their active form are bound to a receptor located in a membrane. We present results here on two important naturally occurring peptide systems using a variety of gas-phase techniques; our data is interpreted with reference to its biological significance.

The gonadotropin-releasing hormone (GnRH) peptides are a family of decapeptides also known as luteinizing hormone releasing hormone (LHRH). They play a key physiological role as a mediator of neuroendocrine regulation in the mammalian reproductive system [12,13]. Of the 23 naturally occurring structural variants of GnRH thus far identified, the N-terminal residues (pGlu-His-Trp-Ser) and the C-terminal residues (Pro-Gly-NH_2) are conserved with a few exceptions [14]. In mammalian GnRH, residues 5–8 are believed to adopt a type $II^1\beta$ turn conformation which allows interaction with GnRH type I receptors [15]. The identity of residue 6 plays a particular role in determining whether this $II^1\beta$ turn conformation is adopted or not [16]. Since single amino acid variations in the primary sequence of GnRH peptides have a significant effect on their interactions with the GnRH receptor [6], we have employed Ion Mobility Mass Spectrometry and Electron Capture Dissociation (ECD) to investigate gas phase conformations of GnRH and three structural variants. Molecular dynamics is used to model their structures such that comparisons may be made to the trends observed experimentally.

The second peptide systems described in this paper are β-defensins. These are members of the antimicrobial peptide family which form an important component of the mammalian innate immune response [17,18]. They possess potent broad-spectrum antimicrobial activity and are predominately expressed at epithelial surfaces. Mature peptides sequences are 30–45 amino acids in length and are both amphipathic and cationic. This net positive surface charge implies an initial electrostatic interaction between the peptide and negatively-charged components of the bacterial cell wall, e.g., lipopolysaccahride (LPS) [18]. β-Defensins exhibit exceptionally low sequence homologies save for conserved cysteines, which form disulfide bridges with specific connectivity (Cys 1–5, Cys 2–4, Cys 3–6). It has been proposed that the disulfide bridges impart a structural core and non-conserved residues on the surface are under selective pressure against rapidly evolving bacteria [19,20]. In direct contrast to this perceived structure–function relationship, Wu et al. [21] have recently demonstrated that the antimicrobial activity of human β-defensin 3 (HBD3) is independent of disulfide bridging whilst the peptide's chemotactic properties do depend on it.

Over 10 years ago a crystallographic study of the human α-defensin hNP3 revealed that it forms a dimer containing a six-stranded β-sheet region [22]. More recent work by Lubkowski and co-workers [23] shows a dimeric form of human β-defensin 2 (HBD2), which is present in a quaternary arrangement in the crystal unit cell. These findings provide evidence for the stability of defensin dimers, but can only fuel speculation about the active forms adopted by this class of compounds. It is worth noting that in the more dynamic environment posed by NMR there is little indication of dimer or other higher order aggregate formation [24]. Our work has focused on exploring the effect of oligomerisation on the activity of β-defensins [25]. In this paper we will summarise our

mass spectrometry findings on these two important classes of peptides.

2. Experimental

2.1. Mass spectrometry

Mammalian GnRH used in this study was obtained from Sigma-Aldrich. Ciona1 variants were synthesised by conventional solid phase methodology and purified by HPLC. All GnRH peptides were examined without further purification and made up at a concentration of 20 μM (H_2O:MeOH:CH_3COOH, 0.49:0.49:0.02) for ECD and at 100 μM under the same solution conditions for ion mobility. β-Defensins were obtained from Albachem (UK) and used without further purification. Electrospray solution and source conditions were the same for accurate mass, SORI-CID and ECD. Defensins were sprayed at a concentration of 50 μM (MeOH:H_2O:CH_3COOH, 50:49:1). Dimeric signal was still observed for Defr1 Y5C peptide on ten fold dilution. Solutions were ionised by electrospray and nano-electrospray, from gold/palladium coated tips (Proxeon Biosystems).

Analysis was conducted on two instruments. Ion mobility experiments were conducted on an instrument in the laboratory at UCSB which has been described in detail elsewhere [26]. Ions drift through a cell pressured to 5 Torr with helium at room temperature and are mass selected prior to detection. Arrival time distributions (ATDs) were collected at room temperature over no more than 5 min for each GnRH variant. ATDs were converted to collision cross sections according to transport theory [27] for comparison with values obtained from modelled peptides structures.

Characterization of the oxidation state of the defensin peptides Defr1, and Defr1 Y5C, was performed using the accurate mass capabilities of a 9.4 T FT-ICR mass spectrometer (Bruker Daltonics) at the University of Edinburgh. Using this instrument, two dissociation methods were applied to the isolated peptides. For Sustained Off Resonance Collision Induced Dissociation (SORI-CID) a given charge state was isolated by sweep excitation and subjected to CID with Argon as the collision gas for 500 ms. To perform ECD on both the GnRH peptides and the defensins, a given charge state was isolated by sweep excitation and subjected to electron irradiation for 50 ms using a barium oxide coated high-surface area (5 mm diameter) dispenser cathode (HeatWave) An experimental pulse sequence which combined ECD and SORI-CID was also employed.

2.2. Molecular modelling using the AMBER force field [28]

The GnRH peptides were built using X-Leap [28]. All amino acids were held at their physiological ionization states. A simulated annealing procedure was employed wherein high temperature dynamics is performed at 800 K, followed by dynamics at decreasing temperatures according to an exponential cooling curve. At 0 K the candidate structure is subjected to minimisation using a steepest descent approach followed by a conjugate gradient algorithm. The minimised structure was then used as the seed for the next run of high temperature dynamics. Three hundred candidate structures were generated of each GnRH variant. Calculations were performed on an Alpha Server Compaq DS20e which forms part of the EPIC bio-computing facility [29]. The two lowest energy structures obtained were then subjected to molecular mechanics for 1 ns at 300 K, to determine the conformational flexibility of the minimised structures. Representative snapshots of co-ordinates obtained during this run are those discussed within the text. These structures were viewed and analysed using VMD [30]. An orientation averaged projection cross section is calculated from each candidate structure geometry, which is scaled according to the temperature dependent helium interaction potential [31].

3. Results and discussion

3.1. GnRH—gonadotropin releasing hormone

3.1.1. Ion mobility studies on mammalian GnRH and Ciona1 structural variants

Results of the measurements made and comparison with model geometries are shown in Table 1. The four peptides here are mammalian GnRH and three structural variants, one of which is the naturally occurring form for the lower non-vertebrate Ciona1 (a type of sea squirt). The other two are mutants of Ciona1 where the sixth residue (shown in bold) has been substituted Ala → Gly and Ala → D-Ala. Primary sequences for the two naturally occurring peptides are shown below:

Mammalian GnRH: pGlu-His-Trp-Ser-Tyr-**Gly**-Leu-Arg-Pro-Gly-NH_2

Ciona1: pGlu-His-Trp-Ser-Tyr-**Ala**-Leu-Ser-Pro-Gly-NH_2

There is good agreement between experiment and theory for all peptides examined with differences within expected experimental error. The number in brackets indicates that a

Table 1
Measured and calculated cross sections for four GnRH variants

GnRH	$[M+H]^+$ (Å^2)		$[M+2H]^{2+}$ (Å^2)	
	Experimental	Calculated	Experimental	Calculated
Mammalian	246.2	249.5 (6)	252.3	253.3 (6)
Ciona1	256.8	257.5 (9)	252.1	254.3 (11)
Ciona DAla(6)	249.9	249.8 (5)	245.8	246.2 (9)
Ciona Gly(6)	247.7	247.6 (8)	243.7	242.4 (3)

Results are shown for both singly and doubly charged ions. Calculated values are an average of the cross sections obtained from candidate geometries which, when all 100 structures are sorted by relative energy occur in the lowest 20%. The numbers in brackets are the standard deviations from this central value.

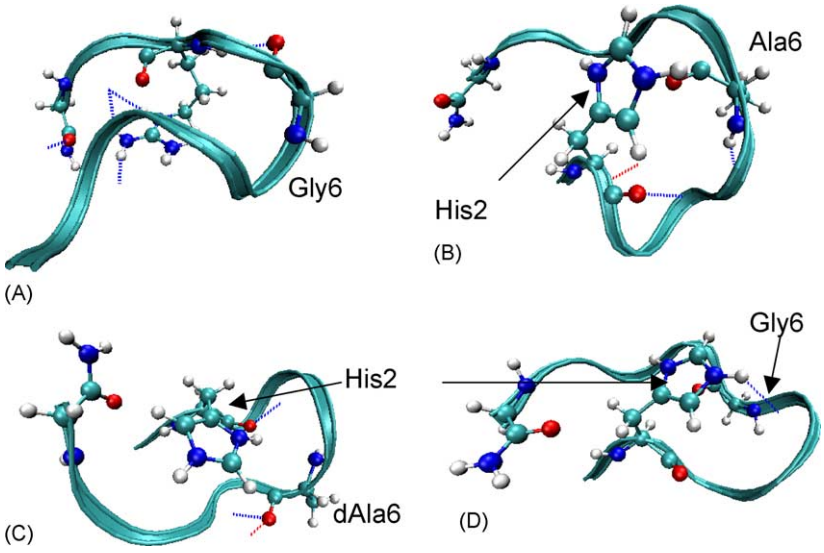

Fig. 1. Representative low energy structures of singly charged GnRH peptides $(M+H)^+$ from molecular dynamics performed at 300 K. (A) Mammalian GnRH, (B) Ciona1, (C) Ciona1DAla6 and (D) Ciona1Gly6. The blue dotted lines indicate hydrogen bonds formed for that conformation. For each peptide, three residues have been depicted in CPK format, for the Ciona 1 peptides these are His2, Ala6/DAla6/Gly6 and the amidated C terminus, for mammalian GnRH these are Gly6, Arg8 and the amidated C terminus.

range of cross sections are found for low energy structures, however, the mean value is close to that found experimentally in each case.

Two major trends are apparent in this data: the first is that the Ciona1 singly charged peptides have slightly larger cross sections than their doubly charged equivalents, but for the mammalian form the reverse is true. The second is that the size order of cross sections obtained for all the forms of GnRH both singly and doubly charged is found to be:

$$\text{Mammalian GnRH} < \text{Ciona1Gly6} \approx \text{Ciona1DAla6} < \text{Ciona1}.$$

These trends are best discussed with reference to the molecular models obtained.

3.1.2. Molecular modelling—the structures

For gas phase peptide ions the amino acid which has the highest gas phase basicity is presumed the first to protonate [32]. Considering the peptides studied here, it is most likely to be Arg 8 for the mammalian form and His2 for the Ciona1 variants. To assign a second proton to the $[M+2H]^{2+}$ ions we assume that His2 will also protonate in mammalian GnRH. In the absence of a second basic amino acid for the Ciona1 variants the next most basic site is the C terminal amide group. These assignments are used in modelling to obtain low energy structures whose calculated cross sections appear in the second and fourth columns of Table 1. In all force field calculations sites of protonation are fixed at the start of measurements however experimentally, and particularly on collisional activation, protons on less basic sites are potentially mobile [33]. The relevance to this study will be discussed later, although the good correlation between experimental and calculated cross sections, suggests that it is not a significant problem with the ion mobility measurements of these structures.

Figs. 1 and 2 illustrate representative structures obtained for structures of the $[M+H]^+$ and $[M+2H]^{2+}$ GnRH peptide ions from molecular dynamics runs at 300 K. In all cases the backbone forms a loop which is stabilised by the presence of hydrogen bonds predominantly from side chain groups to backbone carbonyls. With mammalian GnRH Arg8 provides an excellent 'cap' to the peptide backbone (Fig. 1A). In the Ciona1 variants, this role is taken by His2 (Fig. 1B–D). The presence of the second protonation site at the amidated C terminal glycine allows for additional H bond formation, with carbonyl groups along the polypeptide chain. This bonding is analogous to an effect which occurs from C terminal lysine groups [34]. The effect of these cross chain hydrogen bonds is to tighten the structure, which accounts for the decrease in size from $[M+H]^+$ to $[M+2H]^{2+}$. The capping of the polypeptide backbone can be seen in Fig. 2 for all the Ciona1 peptides. The protonated histidine residue in particular with Ciona1Gly6 (C) and DAla6 (D) is able to interact with groups situated on the opposite face of the polypeptide chain. There is a play off here with columbic repulsion that would occur between the two charged groups, and might be expected to increase the cross section of the doubly protonated ions. However, the Ciona1 decapeptide systems orientate themselves such that coulombic repulsion is not dominant, consistent with the slight decrease in cross section from single to doubly protonated ions.

The difference in the cross sections obtained for the single and doubly protonated forms of the mammalian form follows an opposite trend. Here the protonated guanidinium group forms hydrogen bonds to backbone carbonyl groups as can be seen in Fig. 1A. This bonding fixes the structure and subsequent protonation of the bulky histidine side chain results in charge crowding, angling the imadozole ring away from

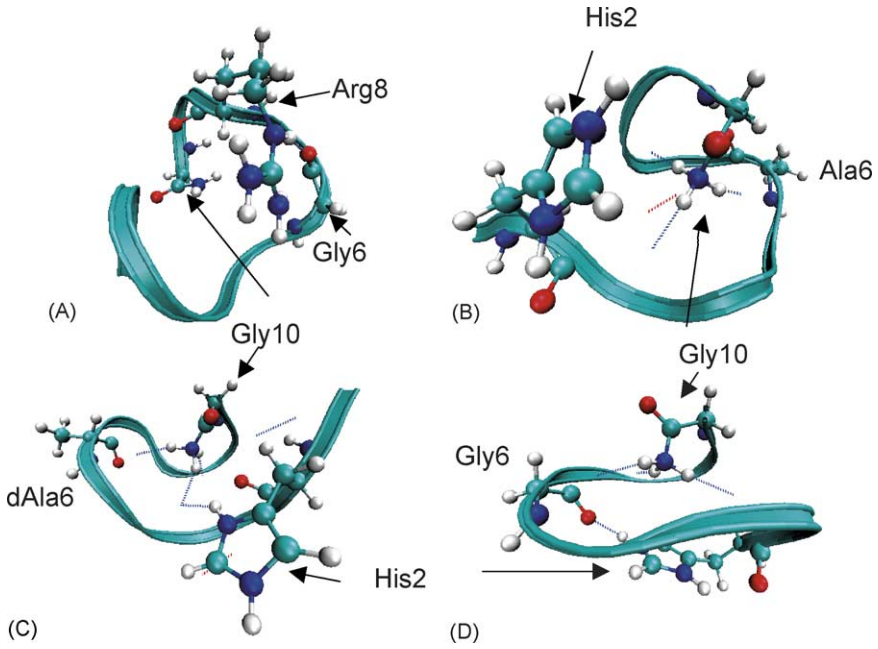

Fig. 2. Representative low energy structures of doubly charged GnRH peptides $(M+2H)^{2+}$ from molecular dynamics performed at 300 K. (A) Mammalian GnRH, (B) Ciona1, (C) Ciona1DAla6 and (D) Ciona1Gly6. The same residues as for the singly protonated peptides are again depicted in CPK format.

the peptide, providing a slight increase in the cross section for the $[M+2H]^{2+}$ ion.

As stated above, for the Ciona1 peptides conformations obtained via simulated annealing are similar. The natural Ciona1 GnRH is somewhat larger than its chiral analogue Ciona1DAla. Cross sections for this DAla6 variant in both charge states are similar to those for the Gly6 variant. This implies that the presence of the D amino acid at residue 6 allows a for a slightly more compact structure which can form a $II^1\beta$ type turn, as with the achiral glycine residue. It appears that the LAla isoform introduces steric hindrance which yields a more open polypeptide than that found in either the DAla or the Gly form. This is supported by molecular dynamics calculations. Fig. 3 illustrates this for Ciona1 and Ciona1Gly6. It can be seen that the distance between residues 3 and 7 (Trp and Leu) is significantly greater in the Ciona1 peptide over the course of a 1 ns dynamics run than that for Ciona1Gly6. Across this defined co-ordinate, which effectively is the diameter of the quasi circular form taken by these peptides, the Ciona1LGly6 $[M+H]^+$ peptide exhibits somewhat higher conformational flexibility than Ciona1. The cross-peptide distance obtained for Ciona1DAla averages at 6.3 Å which falls midway between that seen here for Ciona1Gly6 and Ciona1.

3.1.3. ECD of mammalian GnRH

The use of relative fragmentation intensities to determine gas-phase stability has been employed by many researchers. When examining small molecular systems insights obtained from collision or photo induced dissociation are used with electronic structure calculations, in order to confirm proposed ionic conformations [35,36]. Such approaches rely on accurate knowledge of the process by which fragmentation proceeds. ECD is a relatively new technique, which has principally been applied to determination of primary structures of peptide and proteins [37,38]. Since the precise mechanism of the electron capture and subsequent dissociation process is not yet known, it is difficult to interpret results in terms of the secondary structures of the ions involved. However, we believe that this technique can provide information on gas phase conformations. Polfer [39] has obtained exceptionally reproducible fragmentation patterns from performing ECD

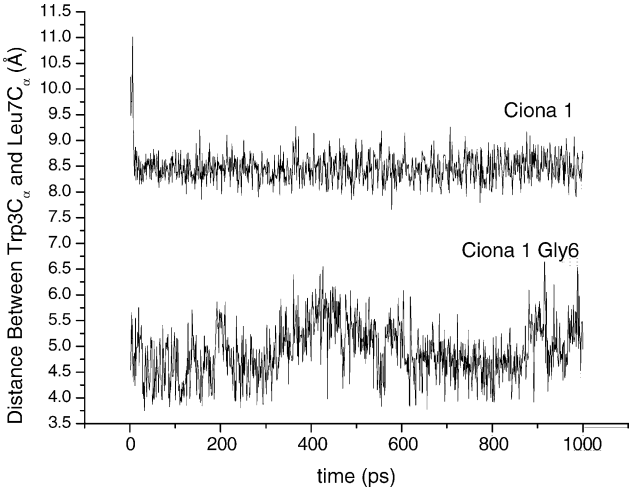

Fig. 3. Co-ordinate plots from molecular dynamics performed on Ciona 1 and Ciona1Gly6. Shown here is the distance between the alpha carbons of residues 4 and 7 over the course of 1 ns of dynamics at 300 K.

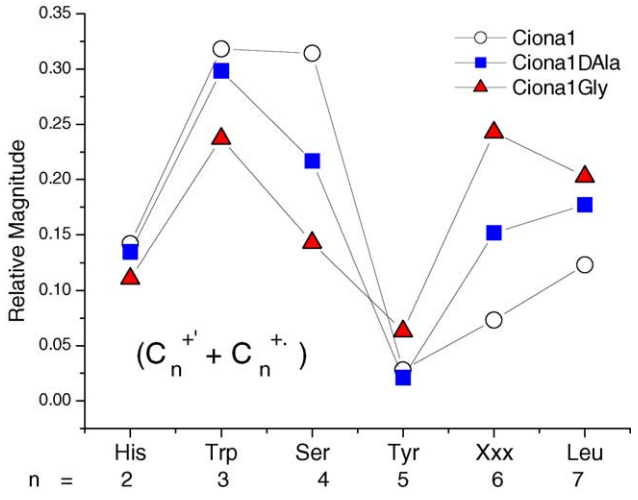

Fig. 4. Relative intensities of ECD fragment ions for Ciona1, Ciona1DAla6 and Ciona1Gly6, each taken from spectra comprising 100 time-domain transients, with 50 ms electron irradiation. The relative intensities are calculated by dividing individual peak intensities by the sum of all the c fragments. Xxx represents Ala6, DAla6 or Gly6.

on a series of GnRH variants. In addition Zuberev and coworkers [40] present evidence for the structural selectivity of ECD by comparing spectra taken from a peptide with a single chiral substitution such as we consider here.

For this study ECD was performed on each of the Ciona1 peptides listed in Table 1. Each peptide yielded partial sequence information from ions corresponding to c_n^+ type fragments, for $2 \leq n \leq 7$. Relative fragmentation efficiencies obtained from each peptide are shown in Fig. 4. For each of the fragments assigned to c_3^+ and c_4^+ ions we also observe ions at masses 1.017 Da lower. These $c^\bullet$ odd electron ions (first reported by Zuberev et al. [41]) occur at intensities which are ~100% of the corresponding c_n^+ ion. For this purpose of this study, c'_n and $c_n^\bullet$ fragments have been summed (Fig. 4). The Ciona1 peptides produced no z-type fragment ions, which implies that charge is retained on the N terminal section of the peptide, presumably due to the higher gas phase basicity of the His2 side chain than that of the C terminal amidated glycine.

Each Ciona1 variant presents a slightly different fragmentation pattern. Error bars, which are not included on this Figure, are within the size of the dots. Both Ciona1DAla6 and Ciona1Gly6, have a lower fragmentation intensity for the c_4^+ channel, than that for Ciona1. This effect is reversed for the c_6^+ channel. This is a significant result. Switching the chirality of the alpha carbon at this residue from Ala → DAla and substitution of the achiral Gly residue yields an increased preference for this fragmentation channel. This strongly suggests that there is a difference in the gas phase structures of these ions, and that the presence of glycine favours capture and cleavage at this position on the polypeptide backbone. A similar effect is seen for the production of the c_7^+ fragment. As might be expected from peptides where 9 out of 10 amino acids are the same, there are also some comparable features. For example, the c_2^+ and c_5^+ product channels appearing at similarly low abundances for each GnRH variant.

Quantitative analysis of this data with reference to gas phase conformation(s) of these peptides is not conclusive. If the ECD mechanism proceeds via electron capture at a proton which is hydrogen bonded to a backbone carbonyl, then it appears that the presence of LAla reduces the formation of such a bond, although two out of the 10 low energy structures examined did show such a bond. Since there is still some fragmentation here for the Ciona1 peptide, it may simply be that the opening of the peptide backbone lessens the likelihood for hydrogen bond formation at this point. The use of force fields to provide gas phase structures is limited by the absence of a parameterised mobile proton. Our calculations have all employed the amidated N terminus as the second protonation site. This choice introduces some flexibility and as can be seen in Fig. 2B–D, where the protonated amidated glycine forms hydrogen bonds to several backbone carbonyls. Whilst our ion mobility measurements support this structure, it is possible that on collisional activation (for example in the transfer hexapole of the FT-ICR) such a proton would be mobile prior to ECD. A proper comparison of ECD data to gas phase structures must consider this.

3.1.4. Biological significance

Many thousand synthetic analogues of GnRH have been made and so the significance of each amino acid in this peptide towards binding at the receptors in the anterior pituitary has been well established in this intense research field [6]. What is clear from earlier work is that the presence of a chiral amino acid at residue 6 significantly reduces binding at the mammalian GnRH I receptor [6,42]. This is presumed to be due to the inability of peptides to form the tight type $II^1\beta$ turn which preconfigures the ligand prior to receptor binding and activation. The structures shown in Fig. 1B and C taken in parallel with the ion mobility results illustrate that the Ciona1 peptide has a looser conformation than the DAla6 or Gly6 structural variants. Some low energy structures for both the mammalian GnRH and the DAla6 and Gly6 Ciona1 peptides do exhibit such a turn at or around residue 6. Data obtained from the $[M + 2H]^{2+}$ ions is less relevant here, since the C terminal glycine is probably not protonated in vivo, however our preliminary ECD results also imply a different gas phase conformation for these peptide ions, which also reflects the influence that single amino acid changes can have on structure. The binding affinity of the Ciona1 peptides will be the subject of a future communication [43].

3.2. β-Defensins

3.2.1. High resolution mass spectrometry of defensins

The sequences of the two defensins examined here are below. They differ by just one amino acid, the substitution of Tyr → Cys forming Defr1-Y5C which contains six cysteines,

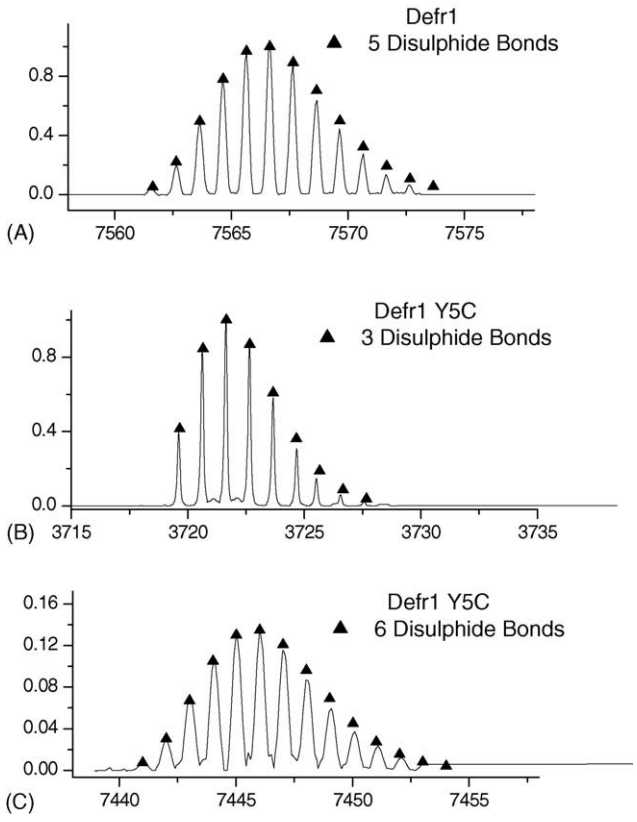

Fig. 5. (A) High resolution mass spectrum of oxidized Defr1 dimeric isoforms. The triangles correspond to the isotopic envelope calculated from the Defr1 amino acid sequence containing five disulfide bonds [46]. (B) Deconvoluted isotopic envelope from FT-ICR nanospray analysis of oxidized Defr1 Y5C. The triangles correspond to the isotopic envelope expected from a Defr1 Y5C monomer with all cysteines oxidized, i.e containing three disulfides. (C) Equivalent spectra for the dimeric form of Defr1 Y5C, here the triangles represent the isotopic envelope expected from a dimer with all cysteines oxidized, i.e., six disulfide bonds [46].

from the five-cystine containing murine defensin Defr1.

Defr1 DPVT $\overset{1}{\mathbf{Y}}$IRNGGI $\overset{2}{\mathbf{C}}$QYR $\overset{3}{\mathbf{C}}$IGLRHKIGT $\overset{4}{\mathbf{C}}$GSPFK $\overset{5}{\mathbf{C}}$ $\overset{6}{\mathbf{C}}$K

Defr1 Y5C DPVT**C**IRNGG**I****C**QYR**C**IGLRHKIGT**C**GSPFK**CC**K

Using FT-ICR mass spectrometry we have been able to unambiguously define the number of cross-linked cysteine residues in each peptide, by comparing the measured isotopic distribution to that expected for a fully or partially reduced species. Since it is possible to reduce cysteine in the electrospray process, accurate mass was performed on defr1 pre-incubated with iodoacetamide. After this treatment, the deconvoluted signal seen from the Defr1 dimer fits the isotopic abundances predicted from its primary sequence (Fig. 5A). In this spectrum the isotopic envelope matches *extremely closely* to that expected for fully oxidized Defr1, ruling out anomalous gain or loss of hydrogen's during the electrospray process, and supports the accurate mass assignment we have made. Interestingly there was no peak corresponding to the monomer of Derf1 + idoacetamide (region not shown), suggesting that no monomer is present in solution prior to mass spectrometric analysis. This strongly implies that Defr1 exists as a dimer linked by an intermolecular disulfide bridge, and that if there is some partially reduced defensin in solution it will be at cysteines which are not involved in the intermolecular disulphide bridge. In short this peptide is dimeric with five disulphide bridges. To further characterize this we employed dissociation techniques including reduction of disulphide by ECD to probe the stability of the defensin peptides in the gas phase.

For Defr1 Y5C the isotopic distribution obtained fits well to that predicted for a fully oxidized monomeric peptide, so we can conclude that this peptide contains three intramolecular disulphide bonds (Fig. 5B). We also observed a Defr1 Y5C dimer which appears to be composed of two non-covalently associated monomers, with all six disulphide bonds formed (Figs. 5C and 6B). Since this mass spectrum was acquired under denaturing acidic nano-spray conditions, and in the harsh desolvation conditions of the Bruker Apex III source, we presume that Defr1 Y5C must form a dimer due to favourable non-covalent interactions, which is the conclusion of others on observation of oligermeric peptides via MS [44]. On lowering the concentration to 5 μM we still observe the dimeric form of this peptide. This tendency to aggregate is also bourn out by gel electrophoresis, which has also revealed a dimeric form of Defr1 Y5C [25].

3.2.2. *Determination of the structural core via CID and ECD*

CID of the Defr1 dimer gives rise to b-type fragments from the N terminus up to the location of the first cysteine (b_2–b_{10}) and a y-type fragment resulting from the loss of the C-terminal lysine, indicating a distinct structural core (Fig. 6A). Some very low intensity species are apparent with masses ±32 arising from monomer units formed by cleavage of the C–S bond of the intermolecular cysteine bridge. The lack of any significant monomeric 'daughter' fragments, demonstrates that the dimer is covalently bound. These findings are further supported by ECD where cleavage of Cys–Cys disulphide bridges is a favoured process [41]. Here this appears to occur preferentially at the intermolecular disulphide bridge leading directly to two monomers (Fig. 7). We can conclude from this, that the intermolecular bridge is accessible for cleavage, at least when this dimer exists as a gas phase ion.

We also performed CID on the Defr1 Y5C dimer and in contrast to Defr1 it readily dissociated into monomers (Fig. 6B and C), supporting the conclusion of the accurate mass work above that this is a non-covalently bound dimer. $b_{2–4}$ fragment ions were observed, corresponding to loss of the shorter N terminal section of this peptide, but as for Defr1, the disulphide bridged core resisted collision induced dissociation.

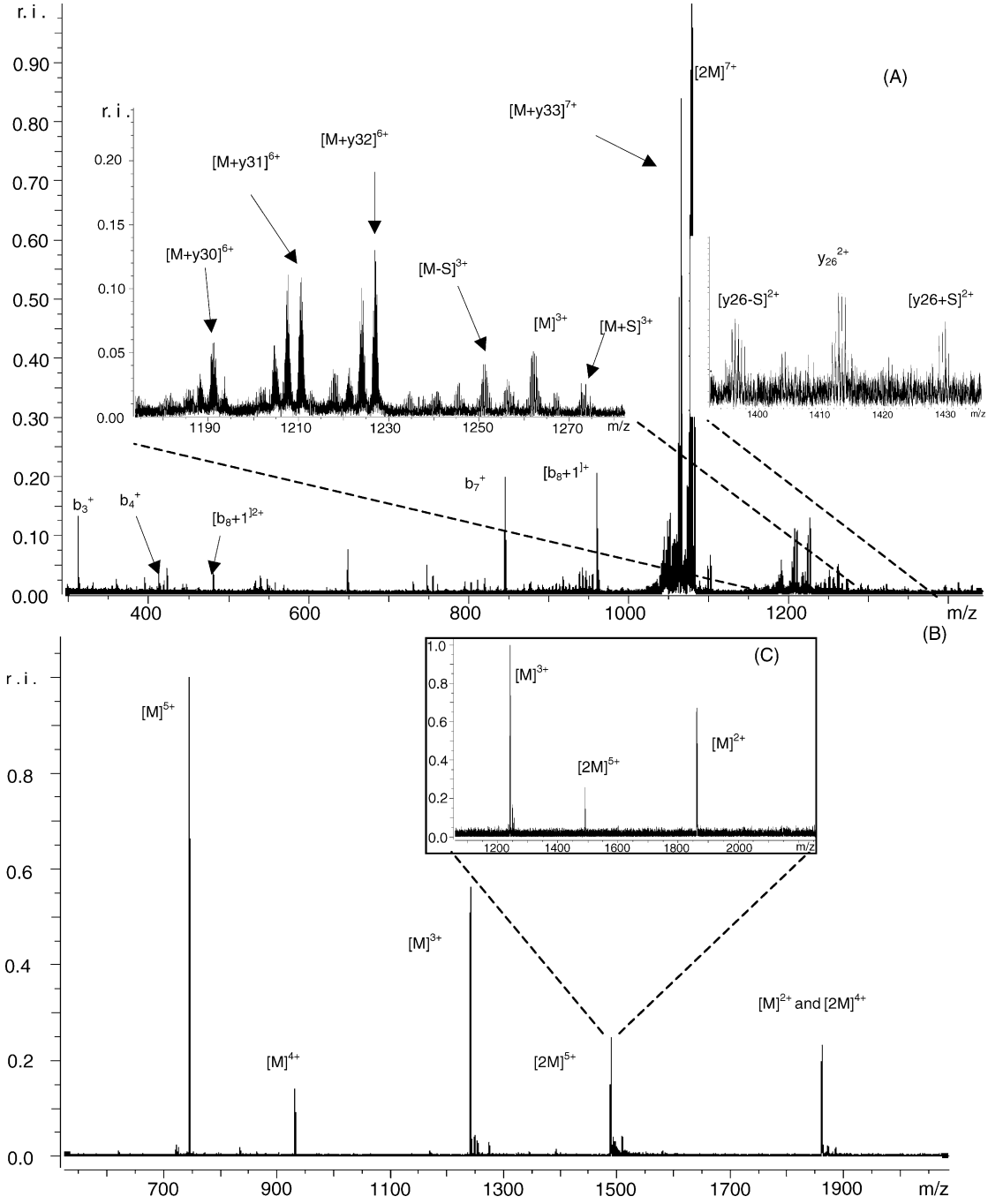

Fig. 6. (A) SORI-CID spectra of Defr1. Charge state +7 (m/z = 1081.401) was isolated and subjected to collisional activation with argon for 40 ms prior to detection. Fragments arising from activation are labeled. (B) Nanospray mass spectrum of Defr1 Y5C taken in acidic conditions. The peak due to the +5 charge state of the non-covalently bound dimer occurring at m/z = 1488.905 (monoisotopic mass) is indicated, as are the peaks arising from the monomer charge state series. (C) SORI-CID spectra of the Defr1 Y5C dimer. The peak at 1488.905 was isolated and subjected to collisional activation. This dissociates readily into two monomeric halves with charge states +2 and +3 as indicated.

3.2.3. Determination of disulphide connectivity's via 'top-down' sequencing and peptide mass mapping

A combination of two dissociation techniques were employed to attempt to discern the disulphide bridging of Defr1: ECD to cleave (selectively) the cysteine bridges and SORI-CID to dissociate the peptide. If sustained ECD alone is used, it is possible to sequence almost the entire peptide however connectivity information is not always forthcoming [45]. The low energy nature of the ECD process employed here, means that for low charge states, even on backbone

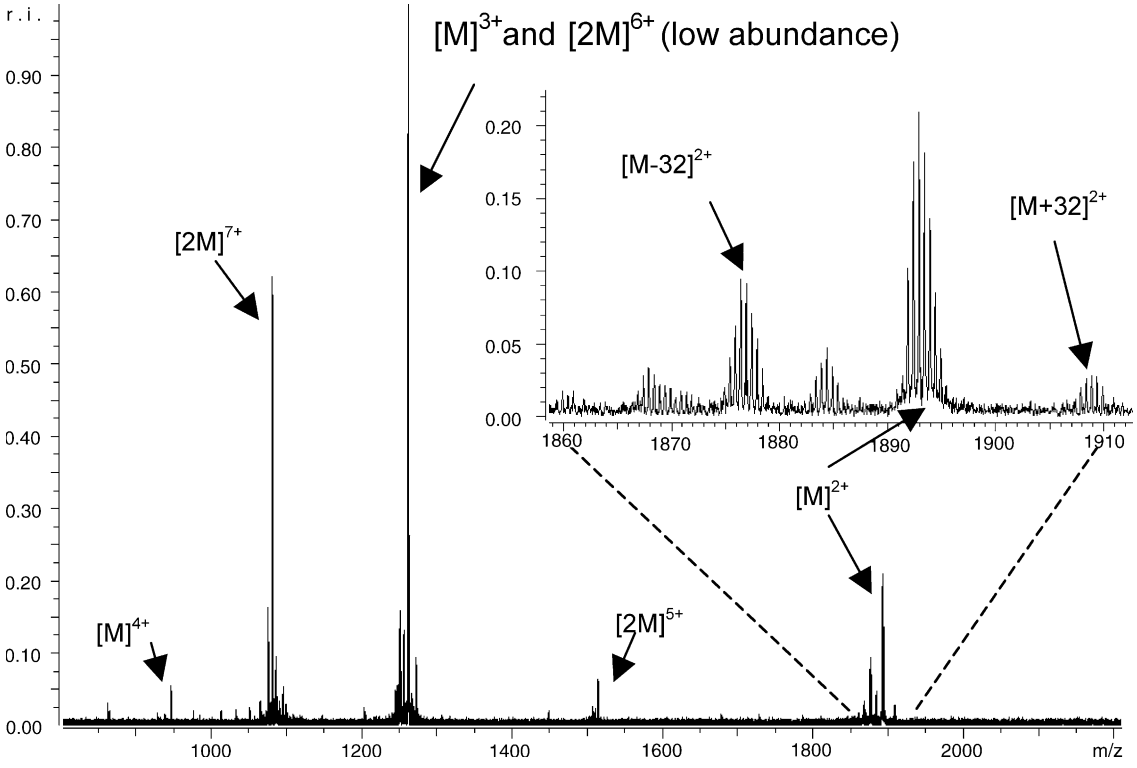

Fig. 7. ECD of Defr1, here the $[D]^{7+}$ dimer ion ($m/z = 1081.401$) was isolated and irradiated with electrons for 50 ms. The +7 ion underwent fragmentation into +5, +4, +3 and +2 monomers. Shown is an expansion of the +2 monomer ion series which results from both symmetric and asymmetric cleavage of the intermolecular S—S bond.

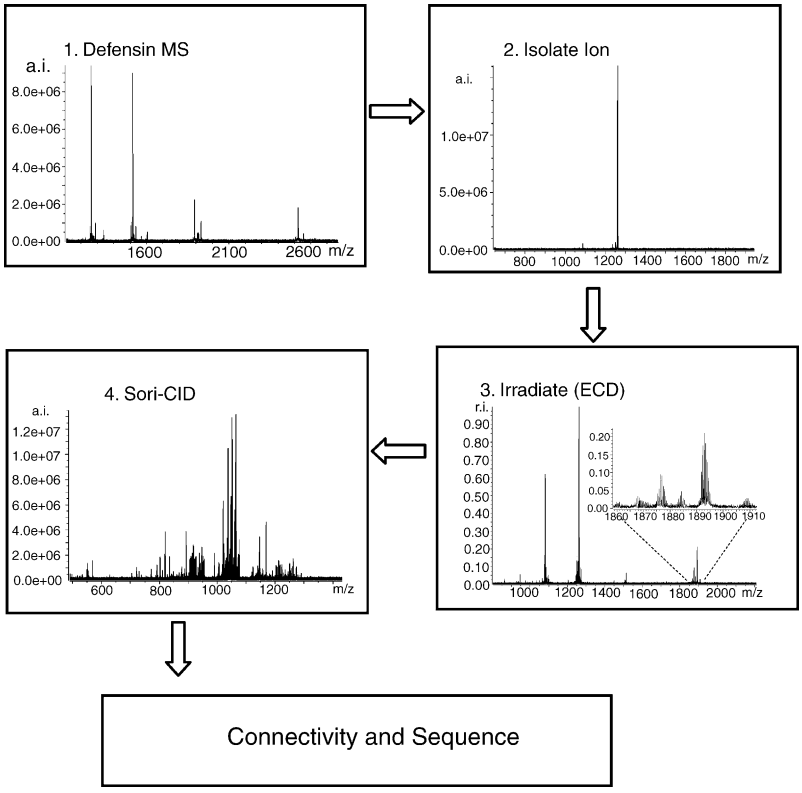

Fig. 8. Strategy for assigning disulphide connectivity using ECD and SORI-CAD.

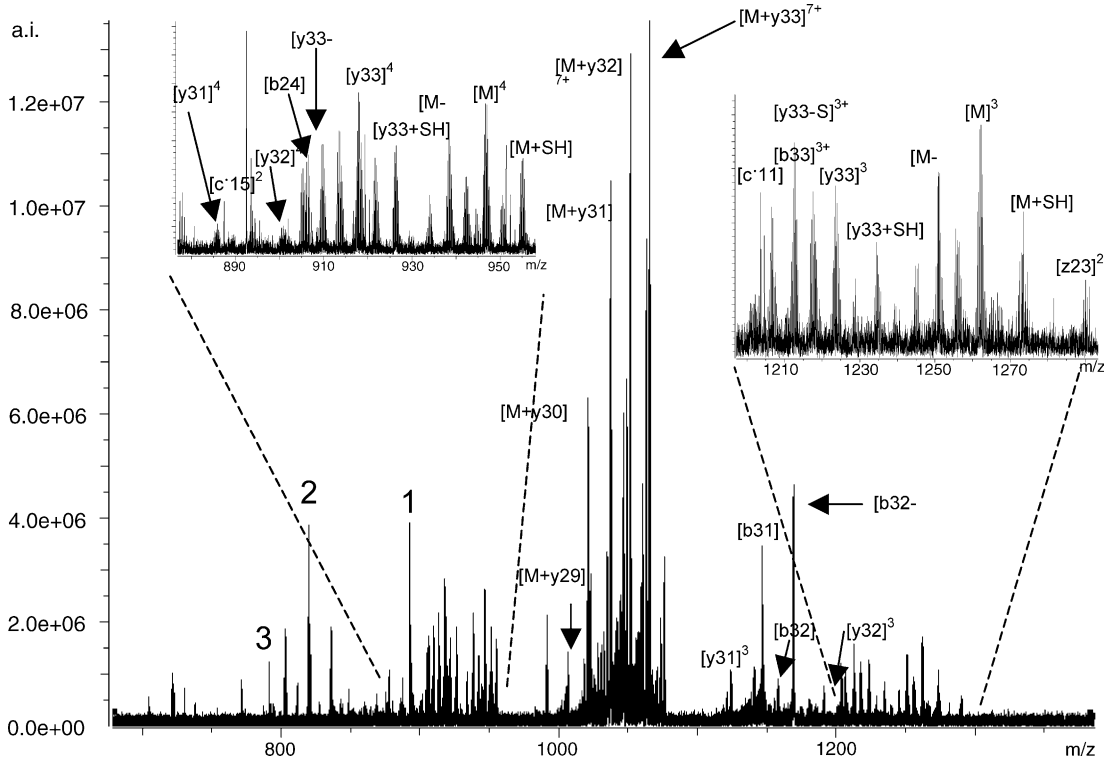

Fig. 9. ECD SORI-CID spectra of Defr1, obtained according to the strategy shown in Fig. 4. Charge states $z = 9$ to $z = 4$ of Defr1 were irradiated with electrons for 50 ms. Then charge state 7 (1081.401 Da) was isolated and subjected to collisional activation with argon for 40 ms prior to detection. Fragments arising from activation are labeled. Peaks 1–3 correspond to internal fragment ions which are described in the text and in Table 2.

cleavage, dissociation into measurable fragment ions does not occur, since non-covalent interactions preserve the gas-phase complex [45]. As stated above, with CID alone cleavage of disulphide bridges is unfavourable and N terminal sequencing to the first cystine only limits the analysis. The strategy which combines ECD and collisional activation is illustrated in Fig. 8.

On isolating the dimeric ion at 1082.797 ($z = 7$) and subjecting it to ECD followed by SORI-CID several fragmentation channels are apparent (Fig. 9). A series of y-type ions ensue from the loss of N terminal amino acids, which are accompanied by water loss peaks. A dominant channel is reduction of the dimer via cleavage of the intermolecular-disulphide bridge, forming monomer ions as described above. Although this also proceeds via cleavage at the thiol ether bond, resulting in signature satellite peaks −32 Da and +33 Da around the dimer. This provides a useful diagnostic of peaks which arise from the dissociation of the dimeric peptide or, of internal disulphide bridges. Table 2 illustrates some of the internal fragment ions which were observed. Isolation and fragmentation of a dimeric ion gives rise to two strong y-type ions which correspond to the loss of CK + S and to CCK from a monomer defensin mass. These peaks are not present if a monomer ion is isolated post ECD and subjected to CID. This indicates that they arise from ECD fragmentation of the dimer ion, into a monomer followed by CID possibly assisted by the location of the Lysine side chain, such that both CID and ECD are directed by the interaction of a protonated site with the peptide backbone [33,37]. The fact that we observe this loss of CK + S only from the dimer, suggests that this arises from a metastable precursor which contains a cleaved thiol–ether bond, and indeed we see such ions (Figs. 7 and 9). The fact that this loss channel is opened to produce the b_{32} + S ion with greater intensity that the b_{32} − S ion indicates a greater stability for the monomer-S species and that is certainly what we see (Fig. 7). Subsequent

Table 2
Internal fragment ions arising from ECD followed by CID, the numbering scheme corresponds to peaks in Fig. 9

Peak number in Fig. 5	ECD/CID fragment residue numbers	Disulphide bridge	Satellite S species	Calculated mass $(M + H)^+$ (Da)	Observed mass (Da)
1	23-31[a] and/or 15-1831-34	4–5 and/or 3–6	Yes	892.44	892.49
2	6-1223-31 and 14-2532-33	2–4 and/or 3–6	Yes	1637.80	819.9217 (2+)
3	15-2033-34	3–6	No	791.41	791.4440

[a] Unlikely to be this internal fragment due to the existence of the satellite S peaks which point to the inclusion of an additional cleaved Cys.

fragmentation gives the b_{31} ion shown by Fig. 5 to be a dominant product. These findings suggest that the intermolecular disulphide bridge is formed between ^{5}Cys–^{5}Cys. This bond is cleaved in some cases asymmetrically which can lead to CID fragment ions which sequence from the C terminus. This process is also dependent on prior cleavage of an internal ^{3}Cys–^{6}Cys bond.

The peaks listed in Table 2 provide evidence for the existence of the internal disulphide bonds 2Cys–4Cys (peaks 1 and 2) and of the internal 3Cys–6Cys bond (peak 3) where no evidence for asymmetric cleavage is found. Elegant though this technique is, we cannot be certain that these are the only connectivities available. An alternative route was taken whereby the two defensins were subjected to proteolytic cleavage, and subsequent peptide mass mapping and sequencing [25]. Data obtained from Defr1 Y5C proved that this six cysteine containing peptide possesses typical β-defensin S–S connectivity (Cys1–Cys5, Cys2–Cys4, Cys3–Cys6). In contrast on digestion, oxidized Defr1 yielded a complex mixture of peptide products. Ions were obtained with masses correlating to Cys2–Cys3, Cys2–Cys4, Cys3–Cys4 and Cys4–Cys4 disulfide bonds, several of which were confirmed by tandem MS sequencing. In short, disulphide connectivity's present in Defr1 are not soley typical of either α or β defensins. Cys2 in particular appears able to form S–S bonds with other cysteine than Cys4. Our conclusion is that Defr1 presents a mixture of topologically different isoforms, rather than a single species with a defined connectivity.

3.2.4. Biological relevance

The activity of these β-defensins against *Pseudomonas aeruginosa* PAO1 was assessed to determine their minimum inhibitory concentrations (MICs) [25]. The MICs were also determined in the presence of the reducing agent dithiothreitol (DTT, 10 mM). The results from our killing assays when taken in tandem with the MS data are remarkable. Defr1 Y5C has identical activity in its oxidized and reduced states supporting the recent conclusions of Wu et al. [21] with HBD3 that disulfide-bonds are not required for β-defensin antimicrobial activity. However, Defr1 is an order of magnitude more active in its oxidized form. This demonstrates that this 10 cysteine containing intermolecular, covalently-linked dimer is a significantly more potent form of this peptide. Defensins are found in high concentrations at cell surfaces [18], and here we have demonstrated the activity of a preformed dimeric species. It is possible that this provides a more effective seed for the formation of higher order aggregates than a monomeric or even a reduced 6 cysteine defensin. Alternatively the presence of the untethered N terminal section of Defr1 may be assisting initial interactions with cell membranes. These observations have implications for the future design of novel anti-microbial agents.

4. Conclusions

The work presented here demonstrates the power of gas-phase techniques in determining peptide structures. Several complimentary methodologies have been applied in order to probe conformational variations in two important peptide systems which arise from single amino acid changes in primary sequences. We have shown how structural variants of GnRH can be elucidated by both ion mobility mass spectrometry and the use of ECD. Molecular modelling has generated structures with cross sections that correspond to those found experimentally. The presence of achiral glycine at residue 6 enables the formation of a tighter structure which assists the binding affinity of this peptide to the mammalian GnRH I receptor. The fact that the gas phase structure can be related to a biologically active form is not entirely surprising, given the lower dielectric medium experienced by a ligand as it binds to a membrane bound protein.

Employing the high resolution capabilities of FT-ICR we have determined the oxidation state of the covalently bound β-defensin dimer Defr1, and developed a strategy which combines ECD and SORI-CAD to map out its disulphide bridging pattern. We have linked the oligomerisation state of a defensin with its antimicrobial activity and these findings imply that there is a critical concentration of this naturally occurring peptide that is necessary to kill bacteria, which is enhanced tenfold by the formation of an intra-molecular disulphide bridge. These findings which have been inspired by collaborations with bio-medical researchers illustrate the potential for solving real biological problems in the gas phase.

Acknowledgements

We would like to thank the Scottish Higher Education Funding Council (SHEFC), Scottish Enterprise (SE), Bruker Daltonics and the School of Chemistry (University of Edinburgh) for funding the world-class facilities of the Scottish Instrumentation and Research Centre for Advanced Mass Spectrometry (SIRCAMS). The Edinburgh Protein Interaction Centre (EPIC) funded in part by the Welcome Foundation, is thanked for use of its computational facilities. In addition we thank the EPSRC (particularly for the award of an Advanced Research Fellowship to PEB) the MRC, the Cystic Fibrosis Trust, the Royal Society and the NSF for funding these studies.

References

[1] R. Aebersold, M. Mann, Nature 422 (6928) (2003) 198.
[2] S. Myung, Y.J. Lee, M.H. Moon, J. Taraszka, R. Sowell, S. Koeniger, A.E. Hilderbrand, S.J. Valentine, L. Cherbas, P. Cherbas, T.C. Kaufmann, D.F. Miller, Y. Mechref, M.V. Novotny, M.A. Ewing, C.R. Sporleder, D.E. Clemmer, Anal. Chem. 75 (19) (2003) 5137.
[3] C.A. Srebalus Barnes, A.E. Hilderbrand, S.J. Valentine, D.E. Clemmer, Anal. Chem. 74 (1) (2002) 26.

[4] T. Wyttenbach, M.T. Bowers, Top. Curr. Chem. 225 (2003) 207 (Modern Mass Spectrometry).
[5] C.A.S. Barnes, M.F. Jarrold, Annu. Rev. Phys. Chem. 51 (2000) 179.
[6] S.C. Sealfon, H. Weinstein, R.P. Millar, Endocr. Rev. 18 (2) (1997) 180.
[7] A. Azmi, R.H. Byrd, E. Eskow, R. Schnabel, S. Crivelli, T.M. Philip, T. Head-Gordon, in: C.A. Floudas, P.M. Pardalos (Eds.), Optimization in Computational Chemistry and Molecular Biology: Local and Global Approaches, Kluwer Academic Publishers, Netherlands, 2000, p. 1.
[8] D.A. Evans, D.J. Wales, J. Chem. Phys. 118 (8) (2003) 3891.
[9] U.H.E. Hansmann, Phys. Rev. E: Stat., Nonlinear, Soft Matter Phys. 70 (1) (2004).
[10] M.J. Pushie, A. Rauk, J. Biol. Inorg. Chem. 8 (1–2) (2003) 53.
[11] B. Turgut, K. Serdar, Biophys. J. 84 (2003) 2871.
[12] J.-K. Chang, A.J. Humphries, R.H. Williams, H. Sievertsson, K. Folkers, C.Y. Bowers, Biochem. Biophys. Res. Commun. 47 (5) (1972) 1256.
[13] M. Fujino, S. Kobayashi, M. Obayashi, T. Fukuda, S. Shinagawa, Biochem. Biophys. Res. Commun. 49 (3) (1972) 698.
[14] R. Millar, S. Lowe, D. Conklin, A. Pawson, S. Maudsley, B. Troskie, T. Ott, M. Millar, G. Lincoln, R. Sellar, B. Faurholm, G. Scobie, R. Kuestner, E. Terasawa, A. Katz, Proc. Natl. Acad. Sci. U.S.A. 98 (17) (2001) 9636.
[15] F.A. Momany, J. Am. Chem. Soc. 98 (10) (1976) 2990.
[16] D.G. Pfleger Kevin, J. Bogerd, P. Millar Robert, Mol. Endocrinol. 16 (9) (2002) 2155.
[17] M. Zasloff, Nature 415 (6870) (2002) 389.
[18] I. Robert, Nat. Rev. Microbiol. 2 (2004) 727.
[19] G.M. Morrison, M. Rolfe, F.M. Kilanowski, S.H. Cross, J.R. Dorin, Mamm. Genome 13 (8) (2002) 445.
[20] C.A.M. Semple, M. Rolfe, J.R. Dorin, Genome Biol. 4 (5) (2003).
[21] Z. Wu, D.M. Hoover, D. Yang, C. Boulegue, F. Santamaria, J.J. Oppenheim, J. Lubkowski, W. Lu, Proc. Natl. Acad. Sci. U.S.A. 100 (15) (2003) 8880.
[22] C.P. Hill, J. Yee, M.E. Selsted, D. Eisenberg, Science 251 (5000) (1991) 1481.
[23] D.M. Hoover, K.R. Rajashankar, R. Blumenthal, A. Puri, J.J. Oppenheim, O. Chertov, J. Lubkowski, J. Biol. Chem. 275 (42) (2000) 32911.
[24] D.J. Schibli, H.N. Hunter, V. Aseyev, T.D. Starner, J.M. Wiencek, P.B. McCray Jr., B.F. Tack, H.J. Vogel, J. Biol. Chem. 277 (10) (2002) 8279.
[25] D.J. Campopiano, D.J. Clarke, N.C. Polfer, P.E. Barran, R.J. Langley, J.R.W. Govan, A. Maxwell, J.R. Dorin, J. Biol. Chem., 2004, in press.
[26] T. Whyttenbach, P.R. Kemper, M.T. Bowers, Int. J. Mass Spectrom. 212 (2001) 13.
[27] E.A. Mason, E.W. McDaniel, Transport Properties of Ions in Gases, Wiley, New York, 1988.
[28] http://www.amber.scrips.edu.
[29] http://www.epic.ed.ac.uk.
[30] W. Humphrey, A. Dalke, K. Schulten, J. Mol. Graphics 14 (1996) 33.
[31] T. Wyttenbach, G. von Helden, J.J. Batka Jr., D. Carlat, M.T. Bowers, J. Am. Soc. Mass Spectrom. 8 (3) (1997) 275.
[32] A.G. Harrison, Mass Spectrom. Rev. 16 (4) (1997) 201.
[33] V.H. Wysocki, G. Tsaprailis, L.L. Smith, L.A. Breci, J. Mass Spectrom. 35 (12) (2000) 1399.
[34] B.S. Kinnear, M.F. Jarrold, J. Am. Chem. Soc. 123 (32) (2001) 7907.
[35] P. Jackson, K.J. Fisher, G.E. Gadd, I.G. Dance, D.R. Smith, G.D. Willett, Int. J. Mass Spectrom. Ion Processes 164 (1) (1997) 45.
[36] G. Akibo-Betts, P.E. Barran, L. Puskar, B. Duncombe, H. Cox, A.J. Stace, J. Am. Chem. Soc. 124 (31) (2002) 9257.
[37] R.A. Zubarev, N.L. Kelleher, F.W. McLafferty, J. Am. Chem. Soc. 120 (13) (1998) 3265.
[38] R.A. Zubarev, Mass Spectrom. Rev. 22 (1) (2003) 57.
[39] N. Polfer, Ph.D. Thesis, University of Edinburgh, 2004.
[40] C.M. Adams, F. Kjeldsen, R.A. Zubarev, B.A. Budnik, K.F. Haselmann, J. Am. Soc. Mass Spectrom. 15 (7) (2004) 1087.
[41] R.A. Zubarev, N.A. Kruger, E.K. Fridriksson, M.A. Lewis, D.M. Horn, B.K. Carpenter, F.W. McLafferty, J. Am. Chem. Soc. 121 (12) (1999) 2857.
[42] M.J. Karten, J.E. Rivier, Endocr. Rev. 7 (1986) 44.
[43] P.E. Barran, R. Roeske, A. Pawson, R.P. Millar, R Sellar, M.T. Bowers, in preparation.
[44] D.L. Smith, Z.Q. Zhang, Mass Spectrom. Rev. 13 (56) (1994) 411.
[45] D.M. Horn, Y. Ge, F.W. McLafferty, Anal. Chem. 72 (20) (2000) 4778.
[46] The elemental composition for Defr1 dimer is C326H518N100O88S10, average mass 7566.9761 Da. The elemental composition of oxidized Defr1 Y5C monomer with three disulfides is C157H254N50O43S6, average mass 3722.4490 Da and a Defr1 Y5C dimer with six disulfide bonds is C314H508N100O86S12, average mass 7444.898 Da.